Extrachromosomal circular DNA is required for yeast stress granule assembly

Natalia A. Demeshkina[1*] & Adrian R. Ferré-D'Amaré[1*]

[1]Laboratory of Nucleic Acids, National Heart, Lung, and Blood Institute, National Institutes of Health, Bethesda, MD, USA

*Address correspondence regarding this manuscript to N.A.D. or A.R.F.

Emails: natalia.demeshkina@nih.gov, adrian.ferre@nih.gov

Abstract

Stress granules are a key cellular response, conserved across eukaryotes, to environmental insults. They arise upon stress-induced reversible stalling of protein synthesis and redistribution of mRNAs from polysomes into these large cytoplasmic ribonucleoprotein condensates. Many cellular pathways lead to formation and turnover of stress granules. Despite research spanning four decades, biochemical analysis of stress granules remains challenging because of their complexity and dynamic nature. Hitherto, stress granules have been studied cytologically, and their composition deduced from candidate protein approaches including immunoprecipitation and proximity labeling. Now, we have directly purified stress granule cores from yeast, relying on their density and size, finding that they are discrete particles with a size distribution peaking at 135 nm. Unexpectedly, we discovered that in addition to diverse proteins and RNAs, stress granule cores contain extrachromosomal circular DNA (eccDNA). These double-stranded DNAs have been found in all eukaryotes, but there is no precedent for a role in membraneless organelle biogenesis. By repurposing CRISPR technology to target DNA in the cytoplasm, we demonstrate that both presence and accessibility of eccDNA are required for stress granule formation in live yeast cells. Our finding reveals an unrecognized link between DNA metabolism and the cytoplasmic stress response, and suggests that sequence-specific eccDNA-mRNA interactions may mediate stress granule assembly.

Introduction

When eukaryotic cells suffer environmental insults, such as oxidative and osmotic stress, nutrient deprivation, UV radiation and heat shock, a universal response is the cessation of most protein synthesis. Then, translationally inactive mRNAs associate with other cellular components into membraneless cytoplasmic assemblies called stress granules[1-4]. Upon stress alleviation, the granules dissipate, and the released mRNAs re-engage in translation[5,6]. Stress granule formation and disassembly, which are conserved throughout eukaryotes, are thought to be cytoprotective[7]. Many pathways converge into turnover of stress granules[7-11], whose dysregulation is linked to a variety of disease states, including neurodegeneration and cancer[12,13]. Stress granules are also critical in anti-viral response[14], and some viruses hijack them as part of their proliferation strategy[15].

Stress granules were first detected by electron microscopy (EM) of heat-shocked tomato cells[16]. Subsequent studies demonstrated their formation in response to other stressors in diverse eukaryotic cells. In most studies, stress granules have been imaged by light microscopy, relying on fluorescently labeled RNA and protein factors identified as components of the granules[17-19]. Collectively, electron and light microscopy studies suggest that stress granules are comprised of a denser core with an estimated dimeter of 150-270 nm, surrounded by a more diffuse shell[6,17,20]. As stress granules contain many proteins with intrinsically disordered regions, it has been suggested that those diffuse shells have properties consistent with liquid-liquid phase separation[12,21].

Stress granules have also been studied employing methods that complement microscopy. Constituents have been identified by proximity-labeling (APEX) experiments[22,23], by knockdown

and knockout using small-interfering RNA[24], and some procedures have been developed in attempts to reconstitute them in cell-free systems[25,26]. Stress granules have been enriched from mammalian and yeast cells by immunoprecipitation[17,27], revealing numerous candidate RNA and protein constituents.

Most studies of stress granules to date have relied on labeling or immunoreactivity of proteins that partition between stress granules and the rest of the cell. Since the targeted proteins exist in both compartments, the deduced composition or functional properties of stress granules are necessarily made ambiguous by other roles or localization of the candidate component proteins. Moreover, the size of stress granule cores places them at the limit of resolution of light microscopy techniques[4]. In order to generate stress granule preparations unbiased by the enrichment of specific candidate constituents, and as a starting point for high-resolution structural studies, we have now developed a new approach for the isolation of stress granule cores from budding yeast. Our method does not rely on immunoprecipitation. Instead, it employs physical properties of stress granules, such as density and hydrodynamic radius, and results in the purification of discrete ribonucleoprotein (RNP) particles whose RNA and protein composition is largely consistent with the results of previous analyses. Our purified stress granule cores are enriched in DNA-binding and chromatin associated proteins. Completely unexpected, we discovered that circular double-stranded DNA molecules are constituents of stress granule cores. Their sequences are consistent with those of eccDNAs, which have previously been characterized in organisms ranging from yeast to human[28-31]. By repurposing CRISPR technology to target cytoplasmic DNA, we demonstrate that eccDNA is integral to yeast stress granules and required for their formation in live cells. Our purification of stress granule cores from yeast cells opens the way to mechanistic and structural analyses of these

large assemblies, and reveals a direct connection between cytoplasmic circular DNA and the protein biosynthesis machinery in the response to environmental stressors.

Results

Isolation of yeast stress granule cores

We developed a new purification of *Saccharomyces cerevisiae* stress granules formed in response to sodium azide treatment[17], which causes oxidative stress by inhibiting respiration. Unlike previous protocols for partial enrichment, which employed centrifugal pelleting, with[17] (Supplemental Fig. 1a) or without[32] immunoprecipitation, our approach was designed to isolate stress granules based on their average size (~ 180 nm) deduced from *in vivo* imaging[17]. To preserve the integrity of large assemblages, cell lysis was performed without detergents, under conditions imitating the dense cytosol milieu (Supplemental Fig. 1b). Stress granules were collected from soluble fractions by following green fluorescent protein (GFP) fusions of the stress granule markers[17] eIF4G or Pab1, which bind to the 5' and 3'-untranslated regions (UTRs) of mRNAs, respectively. To separate translationally active mRNAs (*i.e.*, in polysomes) from other cytoplasmic complexes, we employed sucrose density gradient centrifugation (SDGC) (Fig. 1a). This revealed comparatively low-density, GFP-enriched fractions with large nucleic acids (Fig. 1b). For comparison, we observed similar low-density material when we subjected to SDGC stress granule-enriched material obtained through the protocol of Jain *et al.*[17] (Supplemental Fig. 2). We further subjected SDGC-fractionated material from our purification to size-exclusion chromatography (SEC) using a resin with a nominal exclusion limit of 100 MDa (Supplemental Fig. 1c). The chromatography was performed in the presence of urea, to separate high molecular-weight

components from loosely bound larger and smaller cytoplasmic constituents (Fig. 1c,d). The elution volume of the well-defined absorbance peak was consistently larger than the void volume (V_0) of the column employed, suggestive of discrete particles, rather than amorphous aggregates. Throughout, parallel control purifications were carried out from lysates of cells treated prior to oxidative stress with cycloheximide (CHX). CHX is widely used in stress granule studies because it blocks release of mRNAs from polysomes, and results in concurrent loss of intensity in the fluorescent cytoplasmic foci identified as stress granules[5,17]. Overall, our procedure allowed us to isolate large, translationally inert cytoplasmic particles, free from polysomes, which was not possible using immunoprecipitation-based protocols.

When examined by nanoparticle tracking analysis (NTA), the species we purified shows a size distribution peaking at 135 nm (Fig. 1e), reminiscent of the conclusions of previous structured illumination microscopy analyses, which indicated the diameter of yeast stress granule cores to be 179.5 ± 28.9 nm[17]. Negative-stain transmission EM shows that SDGC-SEC-purified material comprises particles with a size distribution consistent with that detected by NTA, and with irregular but relatively compact shapes (Fig. 1f,g). Some of the observed shape variability could be the result of embedding the specimens in uranyl formate[33]. This characterization indicates that SDGC-SEC-purified species are large particles (Fig. 1g,h) with narrow size distribution and variable shape.

Purified stress granule cores contain characteristic proteins and RNAs

To help establish the identity of the SDGC-SEC-purified particles, we next analyzed their proteome, and compared the results with the proteome of stress granule cores enriched using the

published[17] immunoprecipitation-based protocol. For this comparison, we performed parallel SDGC-SEC purification and immunoprecipitation enrichment protocols starting with the same yeast culture and cell amounts (Fig. 2a), with identical downstream treatments to minimize pitfalls of comparing protein composition when methods differ (Supplemental Fig. 3a,b). This analysis demonstrated a substantial overlap (45%) between the proteomes of SGDC-SEC-purified particles and the immunoprecipitation-enriched stress granules. The former comprises key proteins conserved in stress granules (Supplemental Table 1 and Supplemental Fig. 3c), including, on par with Pab1 and eIF4G, translational helicases eIF4A and Ded1, eIF3s, heat-shock family Ssa ATPases, subunits of the minichromosomal maintenance (MCM) and chaperonin containing tailless (CCT) complexes, and tubulins. Our SGDC-SEC-purified particles lacked eIF2α, which is not required for stress-granule formation in yeast[19], but is a key regulator of stress granule formation in mammalian cells[1]. Pbp1, the yeast ortholog of mammalian Ataxin-2, was sensitive to urea (Supplemental Table 1), suggesting loose association with the SDGC-SEC-purified particles. Interestingly, the helicase Dbp5, a constituent of RNA export granules, was present in the SDGC-SEC-purified particles, but no other hallmark proteins involved in other cytoplasmic RNP-particles, *e.g.,* the THO/TREX-2 complex or processing (P-) bodies[19], were among the hits (Supplemental Table 2).

In addition to proteins involved in RNA localization, transport, and translation, our SDGC-SEC-purified particles contained abundant DNA-binding proteins involved in chromatin organization and remodeling, and telomere length maintenance. Together with ribosomal components, these were the top hits (Fig. 2b and Supplemental Fig. 3d). For instance, RAP1, a small GTPase that transduces a variety of signals and re-localizes to the cytoplasm upon hypoxia and is essential for

telomere maintenance, was highly represented. Histones were also abundant (Fig. 2c and Supplemental Fig. 3e). When their relative abundance was normalized using the signal from the conserved stress granule helicase eIF4A, we found that the ratio of H2A, H2B, H3 and H4 in the SDGC-SEC-purified particles does not conform to that of the canonical nucleosome. Instead H4 is most abundant (Fig. 2c). We performed immunoelectron microscopic imaging of the surface of SDGC-SEC-purified particles from a strain with chromosome-encoded epitope-tagged H3 (Fig. 2d; H3 is the only yeast histone that can be tagged without compromising function). This revealed embedding of H3 in the particles, suggestive of tight association. Overall, the SDGC-SEC-purified particles have a proteome that substantively overlaps with that previously reported for stress granules enriched using the immunoprecipitation-based protocol[17]. However, the SDGC-SEC-purified particles have an unexpected prevalence of proteins associated with DNA, such as histones and chromatin remodelers.

Next, we characterized the RNA composition of our SDGC-SEC-purified particles. In addition, we characterized the RNA composition of the SDGC-SEC fractions from cells treated with CHX and oxidative stress, to control for the stressor effect of CHX (Fig. 2e-h and Supplemental Fig. 4). In all samples from stressed cells, protein coding transcripts were dominant (Fig. 2e,f), with enrichment in oxidation-reduction processes and other metabolic pathways, and responses to chemical stimuli, among other processes (Supplemental Table 3). Comparison of the mRNA-encoded transcriptome of the SDGC-SEC-purified particles with the 2-fold enriched mRNA transcriptome of yeast stress granules obtained through the immunoprecipitation-based method[34] demonstrated substantial overlap (Fig. 2g). While mRNAs with open reading frames exceeding 1500 nucleotides (nt) were reported to be major constituents of the immunoprecipitation-enriched

stress granules, mRNAs of this length comprised only a third of the mRNA transcriptome of SDGC-SEC-purified particles. To examine if this difference could arise from the pelleting steps of the stress granule enrichment by immunoprecipitation, we carried out SDGC analysis on the core-enriched material obtained using that protocol (Supplemental Fig. 1a; Step 5), finding an abundance of polysomes (Supplemental Fig. 4f). Our analysis, therefore, calls into question whether yeast stress granule cores are enriched in mRNAs with longer mRNA coding regions and UTRs.

Consistent with previous reports on yeast stress granules[34], our SDGC-SEC-purified particles also comprise low-abundance, long-noncoding RNAs (lncRNA; Fig. 2h and Supplemental Fig. 4g) whose specific functions in stress response are poorly understood. We find that the majority of lncRNAs originate from the anti-sense strands of protein coding genes (Supplemental Fig. 4g). Notably, differential expression analysis showed considerable up-regulation of lncRNA in controls treated with CHX (Supplemental Fig. 4h,i). Moreover, pairwise correlation between stressed variants and the parallels treated with CHX revealed only moderate differences (Supplemental Fig. 4c), implying that CHX has effects beyond inhibiting mRNAs from entering stress granules. Together, proteomics and RNA-seq analyses imply that our SDGC-SEC-purified particles are authentic stress granule cores.

Stability of purified stress granule cores

Previous studies suggested involvement of G-quadruplexes in stress granule formation[35,36]. Like what was reported earlier for stress granule-enriched material obtained through the protocol of Jain *et al*.[17], our SDGC-SEC-purified particles are relatively stable when exposed to high ionic strength

conditions (Fig. 3a and Supplemental Fig. 5a-c). However, our particles are noticeably destabilized in the presence of LiCl (Supplemental Fig. 5a). As destabilization by Li^+ is a hallmark of G-quadruplexes, we tested two small molecules with documented G-quadruplex specificity: pyridostatin (PDS)[37] and N-methyl mesoporphyrin IX (NMM)[38]. PDS induced dose-dependent fusion of purified stress granule cores (Fig. 3b) that was not largely influenced by LiCl (Fig. 3c). The PDS-induced aggregation was partially suppressed by NMM (Fig. 3d). However, when the stress granule cores were preincubated with NMM, and PDS was later titrated, aggregation ensued (Supplemental Fig. 5d). The susceptibility of stress granule cores to Li^+ and PDS is consistent with the presence of G-quadruplexes.

Previous observations in live cells correlated disassembly of stress granules upon stressor relief with proximity of ribosomes. This also correlates with re-activation of mRNA translation, as evidenced by increase of polysomes and concomitant decrease in free 80S ribosomes[39]. To test if 80S ribosomes can directly disassemble stress granules, we incubated SDGC-SEC-purified stress granule cores, which contain a plethora of various translational factors and helicases, with 80S ribosomes isolated from the same stressed cells (Fig. 3e,f). Remarkably, this resulted in a dose-dependent disassembly of the stress granule cores. Moreover, this reaction was stimulated by ATP.

To determine if ribosomes associated, and if so, in what manner, with the decondensing stress granule cores, we imaged stress granule cores treated with 80S ribosomes and ATP by negative-stain EM. This revealed the presence of ordered arrays of ribosomes suggestive of polysomes (Fig. 3g). The ATP-dependent disassembly of stress granule cores *in vitro* could mimic the translational

re-activation of sequestered mRNAs upon stress relief. Alternatively, the 80S-induced disassembly may recapitulate translation in the periphery of stress granules detected by live cell imaging[40].

Discovery of circular DNA in stress granule cores

The abundance and variety of DNA-binding proteins (Fig. 2 and Supplemental Table 2) in the proteome of the SDGC-SEC-purified stress granule cores suggested that DNA may be present in these particles. Binding of small molecules with preference for DNA G-quadruplexes (Fig. 3 and Supplemental Fig. 5d) would also support this. We therefore subjected our isolated stress granule cores to treatment with RNase H or DNase I, and evaluated their integrity. Remarkably, treatment with either nuclease resulted in decrease or total loss, respectively, of ethidium bromide-stained electrophoretic bands present in the untreated material (Fig. 4a). To further characterize this unexpected component of stress granule cores, DNA extracted from the particles was digested with ATP-dependent plasmid-safe DNase (psDNase), which degrades all linear DNA and single-stranded circular DNA, but does not target intact or nicked double-stranded, circular DNA (Supplemental Fig. 6a). This analysis demonstrated the presence of double-stranded, circular DNA in the purified stress granule cores (Fig. 4b). Negative-stain EM imaging of DNase I-treated stress granule cores revealed striking unfolding, suggesting that DNA is responsible for compactness and structural stability of these particles (Fig. 4c).

Circle-Seq was previously developed for analysis of total extrachromosomal circular DNA (eccDNA) in yeast[28]. We subjected DNA extracted from our purified stress granule cores to Circle-Seq (Supplemental Fig. 6b) and mapped reads to the *S. cerevisiae* reference genome. This revealed coverage of significant part of the genome, independent of yeast strain or growth medium used for

stress granule purification (Fig. 4d). Circle-Seq showed that stress granule cores from the Pab1-GFP strain, which carries the L-A virus (commonly found in laboratory strains), as well as the virus-free JD1370 strain, share some eccDNAs. However, many eccDNAs are unique to stress granule cores from each strain. Additionally, the analysis revealed differences in eccDNA depending on growth conditions (Fig. 4d). Stress granule eccDNAs ranged in size from several hundred bp to kilobases and mapped to coding and non-coding regions on all sixteen chromosomes, as well as the mitochondrial genome. Our Circle-Seq analysis showed prevalence of eccDNAs with sequences derived from repetitive rDNA, retrotransposons (Ty), and telomeric and subtelomeric elements (Fig. 4e,f). Overall, this analysis revealed that yeast stress granule cores contain eccDNAs whose sequences map broadly to the nuclear and organellar genomes.

Circular DNA is necessary for stress granule formation *in vivo*

Previous studies have documented the existence in yeast of eccDNAs with broad genomic coverage[28], similar to what we found in our purified stress granule cores. Therefore, it is possible that eccDNAs are trapped in stress granules during assembly or purification. Alternatively, eccDNA may be functional constituents of stress granules, and therefore required for their formation *in vivo*. To test this, we downregulated the cytoplasmic eccDNA content of yeast cells and examined the effect of this treatment on stress granule formation. For this, we repurposed CRISPR technology developed to target yeast nuclear DNA, to target yeast cytoplasmic DNA instead (Methods and Supplemental Fig. 7). We chose two 20-nucleotide segments from the Ty1 LTR retrotransposon, which is well represented in our stress granule core-derived Circle-Seq reads. These were encoded in one cassette as parts of guide RNAs (gRNA) under two promoters, SNR52 and SUP4 (Supplemental Fig. 7a). To ensure that gRNAs are present in the cytoplasm in

sufficient quantities, the transcription level driven by SUP4 was monitored by following a Mango fluorogenic RNA aptamer[41] connected through a self-cleaving hepatitis delta virus ribozyme at the 3′-end of the gRNA (Supplemental Fig. 7b). We tagged *Streptococcus pyogenes* Cas9 (*Spy*Cas9) with nuclear export signal (NES, $Cas9_{NES}$) or with red fluorescent protein (mCherry) with NES ($Cas9_{NES}mCherry_{NES}$), and controlled *Spy*Cas9 induction with galactose (Supplemental Fig. 7c,d). The expression level of the endonucleases was optimized to be moderate, to reduce the possibility that abundant cytoplasmic *Spy*Cas9 could itself trigger a stress response.

Yeast with an endogenous Pab1-GFP fusion were transformed with plasmids expressing Ty1 gRNAs, and *Spy*$Cas9_{NES}$, or its enzymatically dead variant ($dCas9_{NES}$) (Fig. 5a). Untransformed cells, and yeast expressing active $Cas9_{NES}$ but without gRNAs (*i.e.*, without crRNA and tracrRNA), served as controls. After subjecting them to oxidative stress (Supplemental Fig. 7c), we imaged the different yeast transformants by confocal fluorescent microscopy. This revealed a dramatic disappearance of stress granules (Fig. 5a) in cells expressing gRNAs and either active or inactive ($Cas9_{NES}$ or $dCas9_{NES}$) CRISPR endonucleases. In contrast, both control lines (untransformed, or expressing $Cas9_{NES}$ without gRNAs) showed robust foci, characteristic of stress granules. Therefore, expression of the complete CRISPR machinery (with either active or inactive endonuclease) targeting Ty1-containing eccDNAs, resulted in disappearance of stress granules. We also examined the same cells at higher resolution and with increased sensitivity using Airyscan microscopy (Fig. 5b). This revealed that cells that lost stress granules instead have small fluorescent foci. These small foci were statistically comparably abundant in the cells expressing the enzymatically inactive $dCas9_{NES}$ (Supplemental Fig. 8).

We next examined whether expression of the CRISPR endonuclease, with or without gRNAs, resulted in reduction of eccDNA levels, by performing Circle-Seq on DNA extracted from cellular fractions subjected to the SDGC-SEC protocol from control and CRISPR transformants (Fig. 5c). This showed that expression of active endonuclease with gRNA led to statistically significant decrease in eccDNA levels. There was no statistically significant decrease in eccDNA in cells expressing either the nuclease alone, or the enzymatically inactive endonuclease with gRNAs. Comparison of Circle-Seq reads covering Ty1 loci in cells expressing gRNAs and either $Cas9_{NES}$ or $dCas9_{NES}$ showed a pronounced depletion in the former (Fig. 5d), implying the reduction in eccDNA levels (Fig. 5c) is due to specific targeting by the active CRISPR machinery. Overall, the decrease in eccDNA in yeast expressing active endonuclease ($Cas9_{NES}$) and Ty1 gRNAs correlates with the disappearance of stress granules in these cells (Fig. 5a,b).

We hypothesized that loss of stress granules in cells expressing gRNAs and enzymatically inactive $dCas9_{NES}$ (Fig. 5a,b) reflects disruption of DNA-protein or DNA-RNA interactions essential for stress granule assembly by the nuclease-gRNA complex. Indeed, considerable affinity for double-stranded DNA by *Spy*Cas9 has been previously demonstrated (Supplemental Fig. 9). Moreover, the usage of inactive dCas9 is fundamental to powerful gene modulation technologies including transcriptional repression. To test this, we expressed the chromatin remodeling helicase Chd1, which has high affinity for various forms of chromatinized DNA, in transformants already expressing $Cas9_{NES}$ and Ty1 gRNAs. As with the CRISPR nuclease, Chd1 was placed under galactose control and tagged with NES for cytoplasmic retention. When we examined $Chd1_{NES}$ co-expressing cells by confocal microscopy with Airyscan, we discovered complete restoration of bright stress granule foci (Fig. 5e). We subjected DNA extracted from SDGC-SEC-purified

particles from the CRISPR+Chd1$_{NES}$ transformants to Circle-Seq, and found restoration of eccDNA to levels indistinguishable from those of wild-type (Fig. 5f). Thus, even enzymatically active Cas9 programmed by gRNAs can be displaced from eccDNA by Chd1, and this restores the ability of the DNA to support stress granule formation. Similarly, Chd1$_{NES}$ expression restores stress granule formation in yeast cells expressing inactive dCas9$_{NES}$ and Ty1 gRNAs (Supplemental Fig. 10). Overall, our CRISPR experiments demonstrate that molecular accessibility to cytoplasmic eccDNA is necessary for stress granule formation in *S. cerevisiae*.

Discussion

Using a new purification strategy that relies on their physical properties, we have purified cytoplasmic particles from *S. cerevisiae* that have been subjected to oxidative stress. The size of the particles, their protein and RNA composition[17,34], sensitivity to G-quadruplex binding compounds[35,36], and physical stability in low- and high-ionic strength conditions[17] suggest that the purified particles are authentic stress granule cores. We discovered that the stress granule cores we purified are specifically destabilized by 80S ribosomes in the presence of ATP (Fig. 3e,f). This is the first biochemical reaction reported between stress granules and another large nucleic acid-protein cellular machine, and is consistent with cytological co-localization[40,42] of ribosomes and stress granules during stress and upon its cessation. This reaction provides an entry point to mechanistically analyze the molecular basis of stress granule disassembly, which is currently unknown.

Completely unexpected, analysis of our purified stress granule cores revealed the presence of circular DNA molecules. When sequenced using methodology developed previously to

characterize yeast eccDNA, we find that the double-stranded DNA extracted from stress granule cores is distinct from plasmid DNA, and has the broad genomic coverage with an overrepresentation of repetitive elements that is the hallmark of eccDNA[28,30]. Despite being ubiquitous and highly heterogeneous in sequence and length across all eukaryotic kingdoms, the biological functions of eccDNA remain to be fully understood[29,30]. Studies have linked this type of DNA to aging[43,44] and development of multiple diseases including neurodegeneration and cancer[45]. Because it is thought to be generated through replication errors with accidental, induced, or programmed DNA breakage of genomic DNA followed by homologous or non-homologous end-joining[30], eccDNA has hitherto been assumed to be primarily nuclear, and not recognized as a component of any cytoplasmic ribonucleoprotein condensates. Whether eccDNA molecules are present in other cytoplasmic non-membranous organelles, such as P-bodies or germ granules will be an important subject of future studies.

Our discovery of the requirement for eccDNA for stress granule formation indicates that it must be present in the cytoplasm. This could occur by translocation through the flexible nuclear pore complex (NPC)[46]. Interestingly, the CCT complex, which mediates protein folding and whose subunits are universally conserved elements of stress granules (Supplemental Table 1)[17], has 377 physical and genetic interactions identified in the *S. cerevisiae* database, of which 48% are with nuclear proteins. In metazoans, cytoplasmic accumulation of eccDNA could also result from nuclear envelope breakdown during open mitosis, which is absent in budding yeast. Moreover, stress itself could alter intracellular trafficking and stimulate export of eccDNA from nucleus by nuclear envelope budding mechanism[47]. Regardless of the mechanism, it will be important to

establish whether stress granules employ pre-existing cytosolic eccDNA molecules for assembly, or their assembly is linked to active synthesis or transport of DNA to the cytoplasm.

Our CRISPR-based experiments imply that not only the presence, but also accessibility of eccDNA is necessary for stress granule formation in yeast. The chromatin state of eccDNAs remains largely unknown. A lack of higher-order compaction in oncogenic eccDNA in certain human cancer cell lines has been reported[48], and our data suggest that the eccDNA within yeast stress granules also is in an atypical chromatin state. A non-canonical histone ratio, with H4 being predominant (Fig. 2c), suggests that histones are not primarily in the octameric form in the stress granule eccDNAs. Presence of the MCM complex (Supplemental Table 1), a chromatin remodeler[49], in purified stress granule cores (previously reported as enriched[17]), is also suggestive of an open chromatin-like state, as is presence of histone H2A.Z (Fig. 2c), a hallmark of nucleosome-depleted chromatin regions[50].

The sensitivity of stress granule cores to RNase H (Fig. 4a), a nuclease that degrades the RNA component of RNA-DNA heteroduplexes, could be indicative of the presence of R-loops, in which an RNA strand invades a complementary DNA duplex[51,52]. Our Circle-Seq results show that the eccDNA component of stress granules covers considerable fraction of the genome; thus, many cellular RNAs would have a complementary segment. Conserved stress granule components such as the MCM complex and other helicases could modulate the extent of R-loops[53]. Our results with PDS and NMM (Fig. 3 and Supplemental Fig. 5d), two compounds with high affinity to DNA G-quadruplexes, suggest that quadruplexing is also involved in stress granule spatial organization.

Formation of R-loops and G-quadruplexes within stress granules would be compatible, as the latter often form in guanine-rich regions of single-stranded DNA extruded in R-loops[54].

Our discovery of eccDNA as a constituent of yeast stress granule cores reveals an active role for circular DNA in the cytoplasm. In contrast to other endogenous cytoplasmic DNAs, which are sensed as pathological and eliminated by various degradation pathways[55], our finding demonstrates a pro-survival function for eccDNA. Moreover, eccDNA within stress granules may indicate an unsuspected link between stress response, cell senescence and aging. Our results suggest that partitioning of RNA into stress granules involves base-pairing with DNA, possibly mediated by R-loops and G-quadruplexes. How sequence-specific DNA-RNA interactions are complemented by sequence-independent nucleic acid association and protein-mediated recognition in stress granule assembly is a key future question. Liquid-liquid phase separation has been proposed to govern the dynamics of stress granule shells[3,56]; in contrast, our results suggest that specific molecular recognition is responsible for stress granule core assembly. Our study provides evidence for a hitherto unrecognized intersection of DNA, RNA and protein metabolism in the cytoplasm of a eukaryotic cell. The connection between nuclear DNA, whence eccDNAs arise, and stress granules also opens a new dimension for future research into disease states including neurodegeneration and cancer, associated with stress granule dysregulation and turnover.

Figures

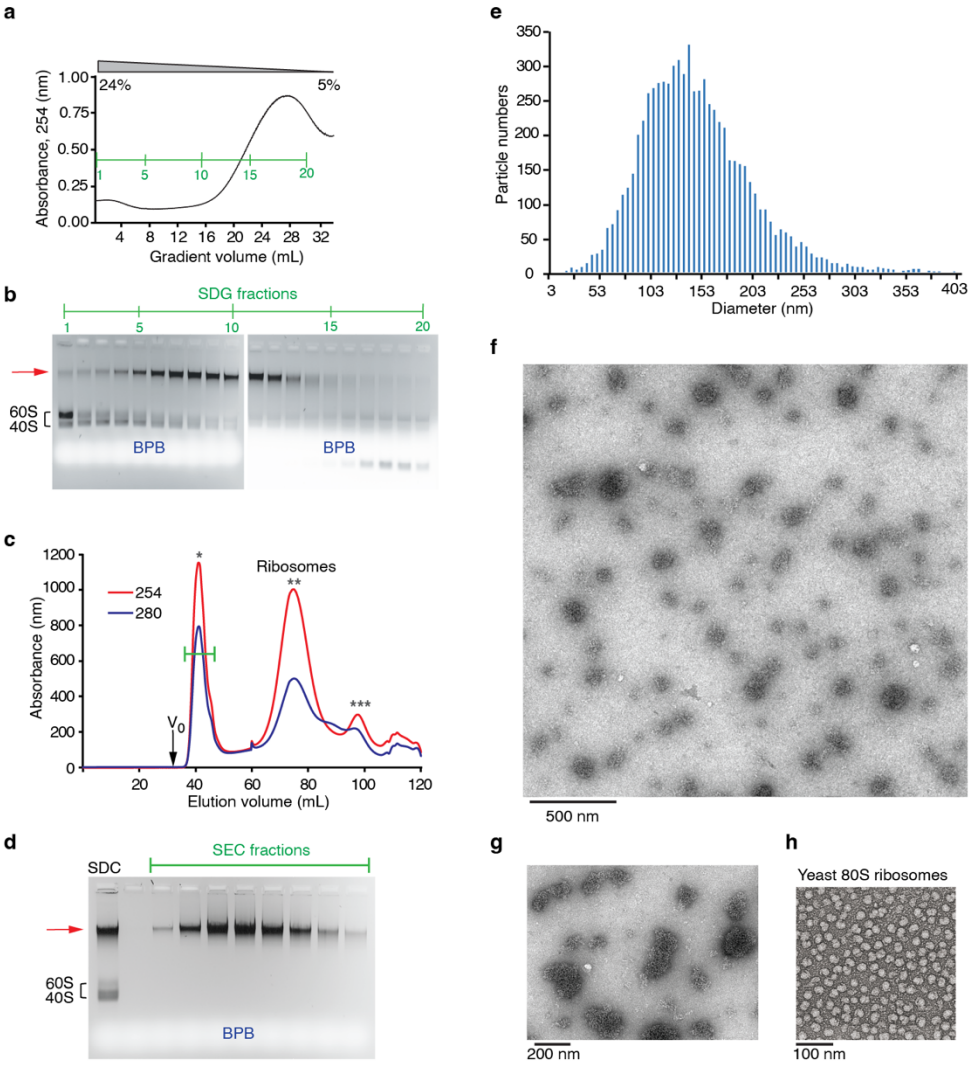

Fig. 1 Stress granule core purification and physical characterization. a, SDGC (5 – 24% w/v) profile of the cytoplasmic fraction of *S. cerevisiae* exposed to oxidative stress. Green line, fractions. **b**, Agarose gel electrophoretic analysis of fractions from **a**. Arrow, electrophoretic mobility of high molecular weight species enriched in nucleic acids. Migration position of 40S and 60S ribosomal subunits and bromophenol blue (BPB) indicated. **c**, SEC of combined fractions 2 – 12 from **a**. Green line, fractions. V_0, void volume. Elution volumes of dextrans of molecular mass $>10^7$, 1.05×10^6 and 43500 Da denoted *, **, and ***, respectively. **d**, Agarose gel electrophoretic analysis of fractions from **c**. **e**, Nanoparticle tracking analysis of the SDGC-SEC-purified particles. The median particle size is 135 nm. **f**, Negative-stain electron micrograph of SDGC-SEC particles (from strain YAG1021). Magnification (× 2,900). **g**, Particles from the same preparation as **f** at magnification (× 6,800). **h,** Negative stain electron micrograph of yeast 80S ribosomes at magnification (× 18,500).

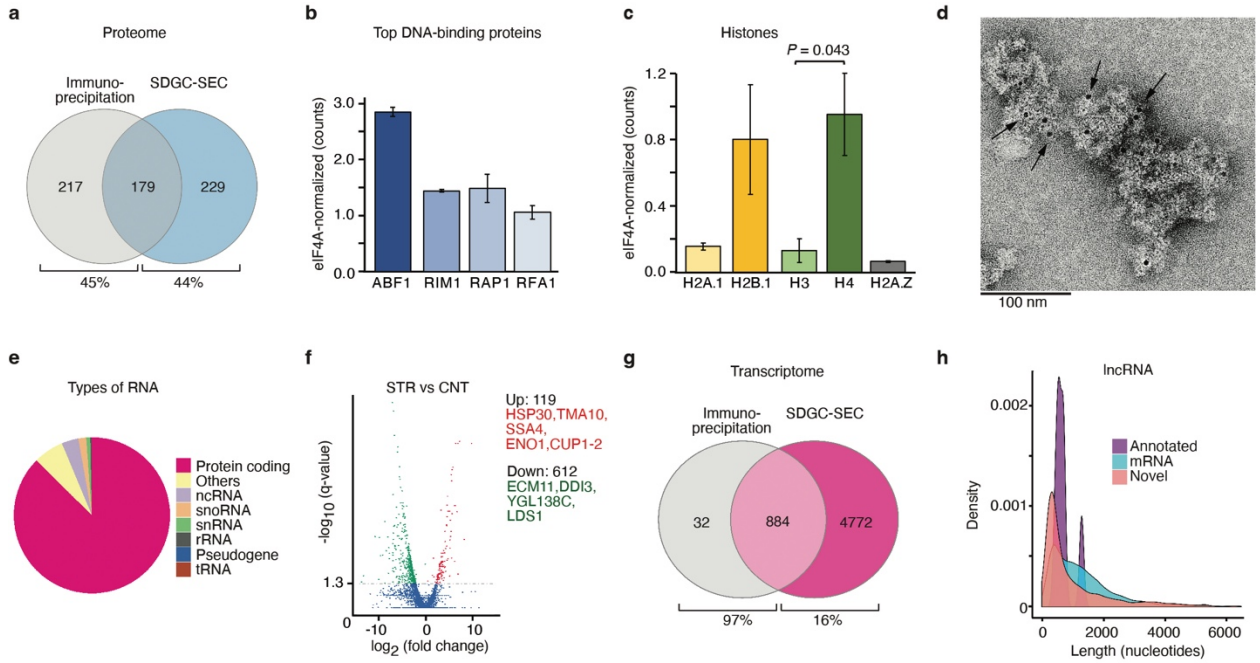

Fig. 2 Proteome and transcriptome of purified stress granule cores. a, Overlap between proteomes of stress granules enriched by immunoprecipitation[17] and the SDGC-SEC-purified stress granule cores. **b**, Top DNA-binding protein hits in the SDGC-SEC-purified stress granule cores (strain JD1370). **c**, Relative abundance of histones identified in the SDGC-SEC-purified stress granule cores. In **b**,**c**, spectral counts are normalized using the counts of the key stress granule protein eIF4A (mean ± SD, $n = 2$ biological replicates, one-tailed t-test). **d**, Negative-stain immuno-electron micrograph of a SDGC-SEC-purified stress granule core(s) from strain YAG1021 carrying a chromosomally encoded FLAG-tagged histone H3. Particles were immuno-labeled with antibodies against FLAG-tag; the antibodies were conjugated to Gold-enhanced NanoGold beads (arrows). Magnification (× 23,000). **e**, Distribution of identified RNA types within SDGC-SEC-purified stress granule cores (strain JD1370). 'Others' category includes lncRNAs with *in silico* coding potential. **f**, Volcano plot for differentially expressed mRNAs from SDGC-SEC-purified stress granule cores from yeast exposed to oxidative stress alone (STR) or to oxidative stress with preceding cycloheximide treatment (CNT) (Supplemental Fig. 4a). Some upregulated (red) and downregulated (green) transcripts are indicated. **g**, Overlap of 2-fold enriched mRNA transcriptome obtained by immunoprecipitation[34] and the SDGC-SEC-purified stress granule cores (strain JD1370). **h**, Distribution of lncRNAs from SDGC-SEC-purified stress granule cores. The majority of detected lncRNAs is unannotated and is shorter than the average length of coding transcripts.

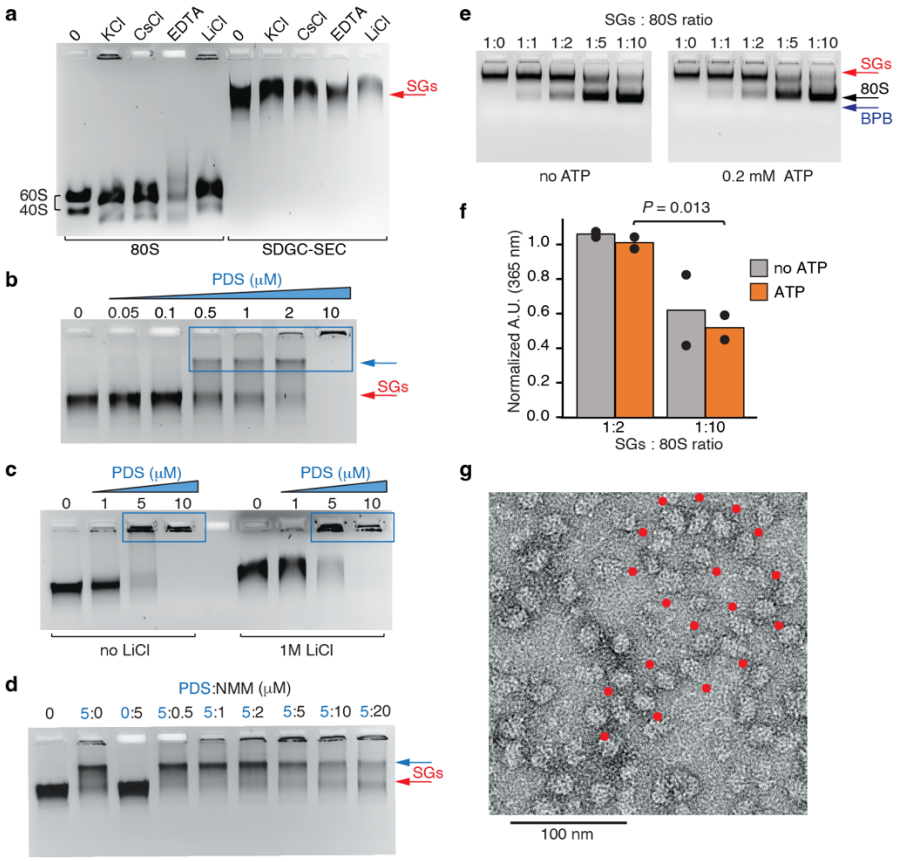

Fig. 3 Chemical and biochemical stability of purified stress granule cores. a, Agarose gel electrophoretic analysis of the stability of SDGC-SEC-purified stress granule cores and 80S ribosomes when incubated with 1M KCl, 1M CsCl, 50 mM EDTA or 1M LiCl. **b**, Interaction of SDGC-SEC-purified stress granule cores with PDS, which specifically binds to G-quadruplex nucleic acids. **c**, Effect of LiCl on PDS interaction with SDGC-SEC-purified stress granule cores. **d**, Interaction of SDGC-SEC-purified stress granule cores with NMM, another G-quadruplex ligand, and PDS. **e**,**f**, Stimulation of disassembly of stress granule cores by 80S ribosomes and ATP. Reactions were analyzed after 35 min incubation at 37°C (mean ± SD, n = 2 biological replicates, one-tailed t-test). In **f**, intensities are normalized with the intensities from the stress granules without additions of 80S and ATP (left lanes in **e**). **g**, Negative-stain electron micrograph of stress granule cores incubated with 80S ribosomes and ATP for 90 min; red dots, likely polysomes. Magnification (× 23,000).

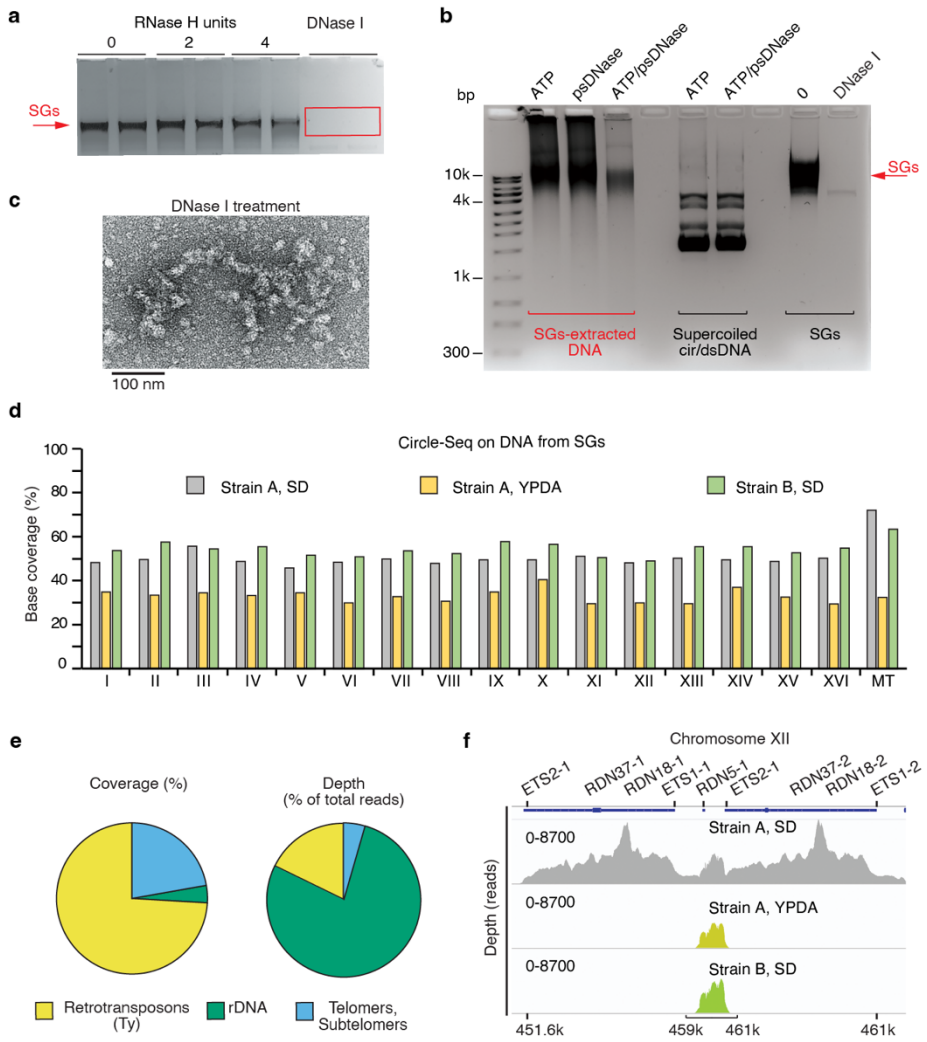

Fig. 4 Circular DNA is a constituent of stress granule cores. a, Agarose gel electrophoretic analysis of SDGC-SEC-purified stress granule cores treated with RNase H and DNase I. **b**, psDNase treatment of DNA extracted from purified stress granule cores reveals circular, double-stranded DNA. Middle lanes, supercoiled intact double-stranded plasmid DNA (control). **c**, Negative-stain electron micrograph of purified stress granule cores treated with DNase I for 30 min at 30°C. Magnification (× 13,000). **d**, *S. cerevisiae* genome coverage derived from Circle-Seq of DNA isolated from purified stress granule cores from strains A (JD1370) and B (YER165W with endogenous Pab1-GFP fusion) grown in rich (YPDA) and synthetic minimal defined (SD) media. Roman numerals denote chromosomes; MT, mitochondrial genome. **e**, Three most abundant classes of circular DNA found in SDGC-SEC-purified stress granule cores. Analysis for strains A and B grown in YPDA and SD media as in **d**. **f**, Circle-Seq reads plotted within rDNA genomic locus demonstrates heterogeneous nature of circular DNA extracted from stress granule cores from strains A and B fermented in YPDA and SD media.

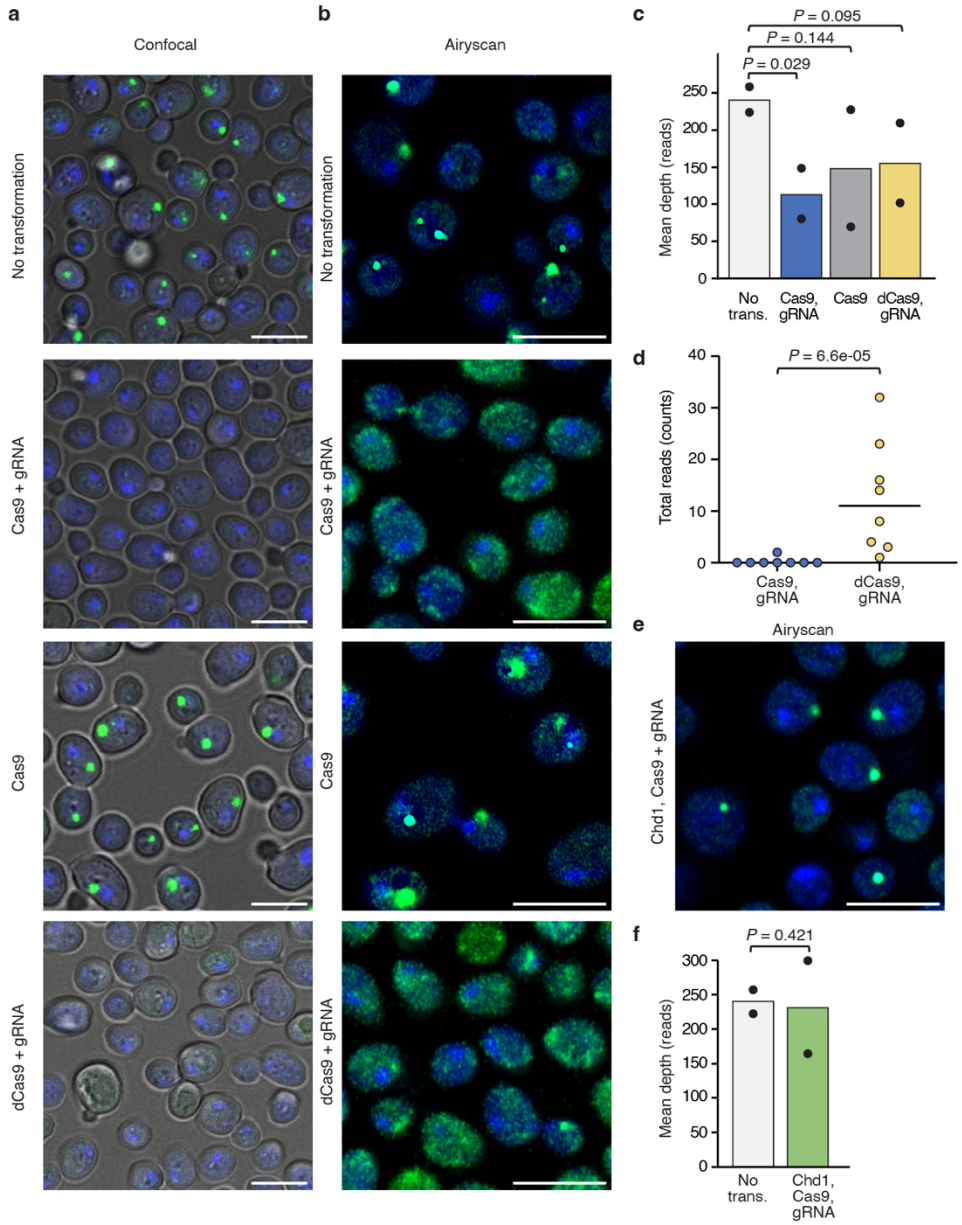

Fig. 5 eccDNA is required for stress granule formation in yeast. a,**b**, Stressed *S. cerevisiae* with endogenous Pab1-GFP and transiently expressed CRISPR machinery. The images were obtained by confocal microscopy without (**a**) or with Airyscan (**b**); CRISPR transformant variants are indicated. Scale bar 10 µm. **c**, Circle-Seq analysis of the effect of CRISPR treatments on total eccDNA content of stress granule cores (n = 2 biological replicates). **d**, Depletion of 20-nt Ty1 ($Ty12^{HDV}$) targets by enzymatically active cytoplasmic *Spy*$Cas9_{NES}$ (3rd generation; Mann-Whitney *U*-test). **e**, Airyscan microscopy of oxidatively stressed *S. cerevisiae* with an endogenous Pab1-GFP fusion and transient co-expression of cytosolic *Sce*$Chd1_{NES}$ and *Spy*$Cas9_{NES}$ with Ty1 gRNAs. Scale bar 10 µm. **f**, Circle-Seq showing effect of *Sce*$Chd1_{NES}$ expression on abundance of eccDNA from stress granules isolated from cells imaged in **e** (mean ± SD, n = 2 biological replicates). One-tailed *t*-tests were used in **c** and **f**. In **a**, **b** and **e**, nuclei were stained with Hoechst

33342 (blue). In **c** and **f**, the ordinates are the mean depth of coverage over all sixteen chromosomes (MT genome subtracted).

Methods

Yeast strains and plasmids

Yeast strains with chromosomally encoded GFP fusions were purchased from the Yeast GFP Clone Collection (Thermo Fisher Scientific). Strains JD1370 (*MATalpha trp1 ura3 leu2 [L-A] [Mi] PEP4::HIS3 NUC1::LEU2*), and YAG1021 (*MATalpha W303 hht2::FLAG-HHT2-URA3*), were kindly provided by Professors J. Dinman (University of Maryland, College Park, MD, USA) and A. Gunjan (Florida State University, Tallahassee, FL, USA), respectively. Plasmids employed for the CRISPR experiments were generated based on the pML104 backbone (Addgene #67638). The pBY011 plasmid encoding yeast CHD1 gene was purchased from the DNASU plasmid repository (clone ID: ScCD00095307). The pBY011 backbone modifications were carried out by GenScript.

SDGC-SEC purification of *Saccharomyces cerevisiae* stress granule cores

A typical isolation started with 6 L of culture. Yeast grown in rich media supplemented with 0.05 g/L kanamycin ($YPDA^{Kan}$) to an OD_{600} of 0.5-0.65 were treated with 0.5% (w/v) NaN_3 for 40-45 min at 30 °C while shaking at 225 rpm. Cells were collected by centrifugation and immediately frozen in liquid nitrogen. Stressed YER165W Pab1-GFP or JD1370 cells yielded 0.8-0.9 g wet weight per L of culture. Control cells were treated with 0.05 g/L cycloheximide prior stress. Cells were thawed on ice, resuspended in modified buffer M (ref.[57]) then recentrifuged, and lysed with glass beads in the same buffer (1 mL buffer/g of cells) supplemented with heparin, protease inhibitors and RNase inhibitors[57]. Lysed cells were centrifuged and the viscous supernatant was

immediately loaded on a 5-24% (w/v) sucrose density gradient and centrifuged in SW 32 Ti rotor (Beckman) overnight. Sucrose density fractions containing large nucleic acids (Fig. 1b) were pooled and centrifugally concentrated. The sample was diluted with modified buffer M and then urea was added to final concentrations of 2 M. The sample was preincubated at 3 °C and loaded on a HiPrep 16/60 Sephacryl S-500 column equilibrated in modified buffer M with 2 M urea (urea was omitted from some preparations). Fractions enriched in stress granule cores were centrifugally concentrated and used immediately or flash-frozen in liquid nitrogen and stored in small aliquots at -80 °C.

Enrichment of yeast stress granules by immunoprecipitation

6 L of yeast culture YER165W-GFP-Pab1 grown in $YPDA^{Kan}$ was stressed and then split equally. For comparison of proteome (Fig. 2a), yeast stress granule cores were either purified as described[17,27] with proportional scaling of all steps to 3 L culture, or by the SDGC-SEC protocol.

Purification of yeast 80S ribosomes

Yeast cells (strain JD1370) were grown and stressed as above in $YPDA^{Kan}$ and used for purification of the 80S ribosomes as described[57].

GFP-fluorescence measurement

Fluorescence of SDGC fractions was scanned using Infinite 200Pro microplate reader and associated i-control 1.9 software (Tecan). The excitation and emission were set at 488 and 535 nm, respectively, with corresponding 20 nm and 25 nm bandwidths. Measurements were carried out in polystyrol black plates (Corning; 25 flashes with 20 μs integration time).

Nanoparticle Tracking Analysis (NTA)

SDGC-SEC-purified stress granule cores were diluted in buffer 2.5/100 [30 mM Hepes-KOH pH 7.5 (at 20 °C), 2.5 mM $Mg(OAc)_2$, 100 mM KOAc, 0.1 mM EDTA-KOH] with 0.5 mM DTT and 80 mM urea, and analyzed using the ZetaVIEW Nano Particle Analysis system (Analytik). The laser and the camera were set at 660 nm and 0.714 µm/px, respectively. A representative acquired track was 7121 traces with 592 average counted particles per frame; two cycles over 11 positions were run. Data were analyzed using ZetaView 8.05.04 software (www.particle-metrix.de).

Electron microscopy

SDGC-SEC-purified stress granule cores (strain YAG1021) were diluted in buffer 2.5/100 (without EDTA and with 1 mM DTT) to 2.0 A_{260} units/mL, incubated at 37°C for 2h, and applied on glow-discharged grids (Electron Microscopy Sciences, FCF300-CU Formvar/Carbon Mesh, Copper; 50 sec at 21 °C). The grids were blotted and treated in 0.1% CWFS gelatin (Aurion) in Tris-buffered saline (TBS) at pH 7.6 for 30 min at 4 °C. Then, the grids were re-blotted and incubated with monoclonal Anti-FLAG M2 antibodies (F1804; Sigma) used at a dilution of 1:30 in TBS for 50 min at 21 °C. Grids were washed three times in TBS for 5 min at 21 °C, and treated with secondary antibodies (#2001; Nanoprobes, 1.3 nm Nanogold-IgG Goat anti-mouse IgG) used at a dilution of 1:50 to 1:100 in TBS with 0.1% CWFG for 45 min at 4 °C. Grids were washed three times as above and stained with freshly prepared 1% (w/v) uranyl formate for 90 sec, and then re-stained for another 50 sec. Images were acquired on a FEI Tecnai T12 transmission electron microscope (Thermo Fisher Scientific). In parallel, grids with yeast 80S ribosomes at A_{260} of 0.25 units/mL were stained with 1% (w/v) uranyl formate for 40 sec at 21 °C and electron micrographs

were obtained. For the 80S disassembly assay, 2.0 A_{260} units/mL of SDGC-SEC-purified stress granule cores (strain YAG1021) were treated with 1 A_{260} units/mL of 80S with 0.2 mM ATP in modified buffer M for 90 min at 37°C. Samples were applied on grids as described above, and stained with 1% (w/v) uranyl formate for 50 sec twice. For localizing FLAG-tagged histone H3 (strain YAG1021), grids embedded with SDGC-SEC-purified stress granule cores and incubated with secondary antibodies (as above) were washed seven times with TBS for one minute. The grids were then gold-enhanced according to the vendor's protocol (Nanoprobes, GoldEnhance EM plus) for 15-20 sec. The grids were washed eleven times for one minute in distilled H_2O and stained with 1% (w/v) uranyl formate for 30 sec; the staining was repeated once more. Micrographs were acquired on FEI Tecnai T12 with a focus on the electron dense gold particles.

Proteomics

1.0 A_{280} unit of SGDC-SEC-purified stress granule cores (from strains YER165W Pab1-GFP or JD1370) was incubated in 1.5 – 2% (w/v) SDS for 30 min at 55 °C with shaking at 300 rpm. Total proteins were extracted with acetic acid, and then precipitated with acetone, as described[58,59]. Pellets of 0.1 mg total protein were further subjected to standard in-solution digestion (disulfide reduction, alkylation and trypsin digestion). To minimize missed cleavage sites, digestion with rLys-C was carried out prior to trypsin treatment. Proteins extracted from the immunoprecipitation-enriched stress granule preparation[17] were treated identically. To compare in-gel and in-solution treatments, proteins extracted from one batch of the SDGC-SEC particles (~ 0.1 mg; strain YER165W Pab1-GFP) were subjected either to in-gel digestion with protein visualization by Pierce Silver Stain for Mass Spectrometry kit (Supplemental Fig. 3) or to in-solution treatment (above). Tryptic peptide analysis was performed using an Orbitrap Fusion

Lumos Tribid mass spectrometer (Thermo Fisher Scientific) interfaced with an Ultimate 3000 Nano-HPLC (Thermo Fisher Scientific). Peptides were fractionated on an EASY-Spray PepMAP RPLC C18 column (2 µm, 100Å, 75 µm x 50 cm) with a 120 min, 5 – 35% (v/v) linear acetonitrile gradient [with 0.1% (v/v) formic acid] at a flow rate of 300 nL/min. The instrument was operated in data-dependent acquisition mode (DDA) using the FT mass analyzer for one survey MS scan on selecting precursor ions, followed by 3 second data-dependent HCD-MS/MS scans for precursor peptides with 2-7 charged ions above a threshold ion count of 10,000 with normalized collision energy of 37%. Survey scans of peptide precursors from 300 to 2000 m/z were performed at 120k resolution and MS/MS scans were acquired at 50,000 resolutions with a range of m/z 100-2000. All MS and MS/MS raw spectra from each set were processed and searched using the Sequest HT algorithm within Proteome Discoverer 2.2 software (PD2.2 Thermo Fisher Scientific). The settings for precursor mass tolerance were set at 12 ppm, fragment ion mass tolerance to 0.05 Da, trypsin enzyme with 2 missed cleavages with carbamidomethylation of cysteine as fixed modifications, deamidation of glutamine and asparagine, oxidation of methionine as variable modifications. The SWISS-PROT *S. cerevisiae* sequence database was used for the search. Identified peptides were filtered for maximum 1% FDR using the Percolator algorithm in PD 2.2 along with additional peptide confidence set to medium. The final lists of protein identification/quantitation were filtered by PD 2.2 (identification set at medium confidence). For the quantitation, a label-free approach was used, where the area under the curve for the precursor ions was used to calculate the relative fold change between different peptide ions. Venn diagrams were created using bioinformatics.psb.ugent.be/webtools/Venn. The GO enrichment was determined using the Yeastmine portal (yeastmine.yeastgenome.org./yeastmine). The relative

quantities of proteins within each dataset were analyzed using the Scaffold proteome software (www.proteomesoftware.com/products/scaffold-5).

RNA Seq

For RNA extraction, SDGC-SEC-purified stress granule cores (strain JD1370) were extensively treated with RNase-free RQ1 DNase and then with RNase-free proteinase K. RNA was extracted with TRIzol reagent (Ambion) according to manufacturer's protocol with additional heating at 60 °C for 20 min. RNA sequencing (high throughput, 33-53 million reads per sample) and analysis were performed by Novogene using the Illumina platform with paired end reads (2 × 150 bp). The quality of RNA was determined using the 2100 Bioanalyzer (Agilent). Ribosomal RNA was removed with the Ribo-Zero Magnetic Kit (Illumina). Clean reads (Q30 > 94%) were aligned to the reference genome for *S. cerevisiae* (iGenomes, Ensembl R64-1-1) using HISAT2 (v2.0.4). Distribution of reads within known RNA types was carried out by HTseq. Assembly was performed by the StringTie package (v1.3.1). Identification of lncRNA was done by screening length and known annotations, and by coding potential using Pfam-scan (v1.3) and CPC (cpc-0.9-r2). Quantification of mRNAs, lncRNAs and TUCPs was assessed by StringTie-eB. Transcript expression analysis was performed by Cuffdiff (v2.1.1) and the GO analysis was performed by running the GOseq (Release2.12).

80S ribosome and ATP-induced stress granule core destabilization assay

SDGC-SEC-purified stress granule cores (strain YAG1021) were incubated at 0.9 A_{260} units/mL with 80S ribosomes at 0.9, 1.8, 4.5 or 9.0 A_{260} units/mL, in the presence of 0.2 mM ATP, in modified buffer M and directly analyzed by electrophoresis on 1% (w/v) agarose(1 × TAE gels

with 1 μg/mL ethidium bromide). Bands corresponding to SDGC-SEC-purified stress granule cores and 80S ribosomes were visualized after a short electrophoretic run; longer runs led to diffusion of SDGC-SEC particle nucleic acids in the agarose matrix and significant reduction in resolution.

Interaction with G-quadruplex-binding compounds

SDGC-SEC-purified stress granule cores (strain JD1370) were incubated at 0.3 A_{260} units/mL in modified buffer M in the presence of 0.05, 0.1, 0.5, 1, 2 and 10 μM pyridostatin (PDS; Tocris Bioscience) for 30 min at 30°C. To investigate the combinatorial effect of PDS and LiCl, the stress granule cores were first incubated with 1.0, 5.0 or 10.0 μM PDS for 20 min at 30°C; then LiCl was added to 1M, and the treatment continued for an additional 30 min. To investigate the combinatorial effect of PDS and N-methyl mesoporphyrin IX (NMM; Frontier Scientific), stress granule cores were incubated with PDS at 5.0 μM and NMM at 0, 1.0, 2.0, 5.0, 10.0 or 20 μM in buffer 2.5/120 for 30 min at 30 °C. All samples were analyzed by electrophoresis in 1% agarose gels as above.

Analysis of stress granule core stability in high ionic strength

SDGC-SEC-purified stress granule cores (strain JD1370) or 80S ribosomes were incubated at 0.6 and 3.0 A_{260} units/mL, respectively, in modified buffer M supplemented with either 1.0 M KCl, 1.0 M CsCl, 50 mM EDTA or 1.0 M LiCl for 1 h at 30 °C. Controls were incubated in unsupplemented buffer 2/150. Samples were analyzed as described above except using a longer electrophoretic run to resolve 60S and 40S ribosomal subunits.

Analysis of stress granule core stability with nucleases

SDGC-SEC-purified stress granule cores (strain JD1370) were incubated at 0.23 A_{260} units/mL with 2 or 4 units of RNase H (10786357001; Roche) in 40 µL of RNase H buffer (20 mM HEPES-KOH pH 8.0, 50 mM KCl, 10 mM $MgCl_2$, 1 mM DTT) or with 1 unit of RQ1 DNase (Promega; RNase-free) in 40 µL of RQ1 buffer (40 mM Tris-HCl, pH 8.0, 10 mM $MgSO_4$ and 1 mM $CaCl_2$) for 2 h at 37 °C. Plasmid-safe ATP-dependent DNase treatment was carried out according to the manufacturer's protocol (Epicenter, Lucigen) with using 1 µg of total DNA extracted from SDGC-SEC-purified stress granule cores and 3 units of the enzyme per reaction. All samples were analyzed by 1% agarose gel electrophoresis as described above.

Circle-Seq

0.3-0.5 A_{260} units of SGDC-SEC-purified stress granule cores (strains JD1370 and YER165W Pab1-GFP) were subjected to digestion with RNases A and T1, and then with thermostable proteinase K with addition of SDS to 1% (w/v). DNA was further extracted using the TRIzol reagent (Ambion) according to the manufacturer's protocol, and then was cleaned using the DNA Clean & Concentrator kit (ZymoResearch). DNA samples were prepared for Circle-Seq as described[28] with the following modifications (Supplemental Fig. 6b). Instead of the restriction endonuclease *Not*I, initial digestion of DNA extracted from SDGC-SEC-purified stress granule cores was performed using exonuclease VIII (truncated, New England Biolabs; 20-30 units per µg of DNA) from 4 to 15 hours at 37 °C. For Circle-Seq of the CRISPR treatments and controls (Fig. 5) exonuclease T (New England Biolabs; 20 units per µg of DNA) was then added, and samples were further incubated for 16-17 hours at 25 °C. Reactions were quenched by heating at 70 °C for 30 min, and DNA was cleaned using the DNA Clean & Concentrator kit. Next, DNA was

extensively treated with ATP-dependent plasmid-safe DNase as described[28]. Finally, 5 μL of each reaction mixture was used for amplification with the REPLI-g kit (Qiagen) at 16 °C overnight and cleaned with the DNA Clean & Concentrator kit to yield samples for sequencing. Circle-Seq was performed by Genewiz (Azenta Life Sciences) using the Illumina MiSeq 2 × 250 bp paired-end sequencing platform. Samples were sequenced to 400-600 Mb. After quality control, reads were trimmed, and low-quality bases were removed (Trimmomatic 0.36). Reads were mapped to the S288C reference genome using the BWA package (0.7.12). Mapping to multiple regions of the genome was allowed to collect information about repetitive regions. Analysis of chromosomal (cumulative: I-XVI) coverage was carried out with subtraction of regions for URA3 (chr V: 116091-117045), the GAL1 promoter (chr II: 278565 – 279010), rDNA (chr XII: 451426-468907) and RPL4B (chr IV: 471853 – 472941) (Samtools (v.1.17), Bedtools (v.2.30.0); properly paired reads only; Fig. 4). Analysis of mean depth of coverage (cumulative: I-XVI) was performed with subtraction of regions for URA3, GAL1, rDNA as above and Chd1 (chr V: 505392 - 509798) (all reads considered; Fig. 5).

CRISPR experiments

The MEME-1 suite[60] identified retrotransposons (Ty) group as overrepresented within Circle-Seq datasets. Candidate 17-20-mers flaked by the 'NGG' protospacer adjacent motif were chosen for targeting two sequences Ty11 and Ty12. Plasmid pML104[61] (Addgene #67638) carrying *Spy*Cas9 under the GAP promoter and nuclear localization signal (NLS, SV40) at the C-terminus was used as a backbone for creation of three variant plasmids where GAP was swapped to inducible GAL1 promoter, and NLS changed to a strong nuclear export signal(s) (NES)[62]. Standard cloning techniques including different restriction enzymes (refer to the pML104 map), Gibson assembly

(New England Biolabs), and QuikChange Lightning site-directed mutagenesis (Agilent Technologies) were used to create: (i) a control plasmid without gRNAs (*i.e.*, without crRNA and tracrRNA), (ii) a full CRISPR system with active Cas9 and gRNAs targeting Ty1, and (iii) a full CRISPR system with dead Cas9 (dCas9) carrying D10A and H840A mutations, and gRNAs targeting Ty1. For the second and third variants of pML104, two cassettes for expression of target RNA (crRNA) were cloned in. The first targeting RNA (Ty11) was cloned under SNR52[61], and the second cassette targeting Ty12 was designed utilizing the approach of[63] where the 3′-end of the gRNA was fused with the self-cleaving HDV ribozyme[64] with inserted Mango-III(A10U) aptamer[41]. The pBY011 plasmid encoding yeast CHD1 gene under the GAL1/10 promoter was obtained from a DNASU plasmid repository and altered by GenScript, where FLAG tag and NES-NES sequences were added to the N- and C-termini of the gene, respectively. All yeast transformations were performed using the lithium-acetate protocol[65] with pretreatment of cells with DTT[66]. Cells carrying plasmid(s) were selected on synthetic defined (SD) yeast solid media with kanamycin and 2% (w/v) D-(+)-glucose lacking uracil (SD(-URA)Dex; 30 °C for 3 days). All transformants were reselected at least once. For each transformed variant, yeast cultures were started at OD_{600} of 6 x 10^{-3} in 10 mL of the SD(-URA)Dex media and grown at 30 °C at 220 rpm until OD_{600} of 3. The cultures were further diluted in the same media and continued to grow until OD_{600} of 2-3. The cells were collected by centrifugation and grown overnight in SD(-URA) containing 1.5% w/v D-(+)-glucose and 0.75% w/v D-(+)-galactose [SD(-URA)Dex-Gal] to express *Spy*Cas9 moderately. Experiments with untransformed YER165W Pab1-GFP were carried out in the identical manner except for inclusion of uracil to the SD media. Overnight cultures were diluted, grown to OD_{600} of 0.3-0.35 in pre-warmed to 30 °C SD(-URA)Dex-Gal and passed through one doubling time (~ 4 h) followed by immediate oxidative stress (40 min at 225 rpm)

with addition of NaN_3 directly to the cultures to 0.5% (w/v) final. Cells were fixed with 4.5% (v/v) formaldehyde for 40 min at 21 °C while shaking at 100 rpm, and collected by centrifugation. Yeast pellets were washed with ice-cold 100 mM K-phosphate, pH 6.5, incubated on ice for 10 min and re-centrifuged; washing was repeated once. Finally, cells were dissolved in 1 × PBS, pH 7.4 and analyzed by confocal light microscopy. For purification of CRISPR SDGC-SEC-purified stress granule cores, the scale of yeast fermentation was 2-3 L per variant of choice. Isolations were as described above, and always run in parallel.

Fluorescence microscopy

Fixed cells were immobilized on concanavalin A or poly-L-Lysine (MP Biomedicals) (for spheroplasts, see below) coated eight-well chamber cover glass (#1.5 high performance, Cellvis). Excess 1 × PBS was aspirated, immobilized cells were washed 2-3 times with 1 × PBS, and stained with 1 μg/mL Hoechst 33342 (ThermoFisher) to visualize DNA. A Zeiss LSM 880 (AxioObserver) workstation with Airyscan was used to conduct optical microscopy experiments. Images were acquired with a Plan-Apochromat 63×/1.4 Oil DIC M27 objective. Confocal microscopy without Airyscan function was carried out with the line-sequential option. Scans were acquired in channel 1 of 488 nm laser, and channel 2 of 405 nm laser. Expression levels of a Cas9 version tagged with mCherry were checked in channel of 561 nm laser. When used, acquired Airyscan Z-stacks (0.3 μm depth) were processed by Zen Black software in 3D mode. To check expression levels of gRNA under stress conditions, strain JD1370 without any fluorescent fusions was transformed with plasmid pML104-GAL1-$Cas9_{NES}$-Ty1-MIII encoding gRNA-2 with the RNA aptamer Mango-III(A10U)(see above). Second generation transformants [SD(-URA)Dex] were grown for 24 h to OD_{600} of 5-7 at 30 °C while shaking at 220 rpm, then diluted and grown in

the same non-induction media SD(-URA)Dex to OD_{600} of 0.7-0.8. Cells were collected by centrifugation at 16000 × *g* for 30 sec, and dissolved in induction media SD(-URA)Gal with 2% w/v D-(+)-galactose. After overnight growth, cells were diluted in appropriate media, cultured (10-20 mL) to OD_{600} of 0.45-0.65 and stressed as above with 0.5% (w/v) NaN_3 for 30 min at 30°C while shaking at 225 rpm. Untransformed strain JD1370 was used as a control. The control parallels were fermented and carried out in the manner identical to experiments except for inclusion of uracil to the SD media. Cells were fixed and washed as above. The cell pellets were resuspended in 1 mL of ice-cold 1M Sorbitol in 50 mM potassium phosphate, pH 7.5. Cell walls were digested with zymolyase (ZymoResearch) following the manufacture's protocol. Spheroplasts were collected by centrifugation at 1000 × *g* for 6 min at 21 °C, then dissolved in buffer A [30 mM potassium phosphate, pH 7.5 (at 20 °C), 140 mM KCl, 1.5 mM $MgCl_2$, 1M Sorbitol] and centrifuged at 1000 × *g* for 10 min at 21 °C. The washing procedure was repeated. Finally, spheroplasts were gently dissolved in 0.2 mL of buffer A and stored on ice (up to 2 days). Prior to imaging, biotinylated TO1 fluorophore[41] was added to 200 nM and fluorescent micrographs were immediately acquired using LSM 880 with Airyscan (laser: 488 nm; see above).

References

1. Kedersha, N. L., Gupta, M., Li, W., Miller, I. & Anderson, P. RNA-binding proteins TIA-1 and TIAR link the phosphorylation of eIF-2 alpha to the assembly of mammalian stress granules. *J. Cell. Biol.* **147**, 1431-1442 (1999).
2. Ivanov, P., Kedersha, N. & Anderson, P. Stress Granules and Processing Bodies in Translational Control. *Cold Spring Harb. Perspect. Biol.* **11** (2019).

3. Protter, D. S. W. & Parker, R. Principles and Properties of Stress Granules. *Trends Cell. Biol.* **26**, 668-679 (2016).

4. Glauninger, H., Wong Hickernell, C. J., Bard, J. A. M. & Drummond, D. A. Stressful steps: Progress and challenges in understanding stress-induced mRNA condensation and accumulation in stress granules. *Mol. Cell* **82**, 2544-2556 (2022).

5. Kedersha, N. et al. Dynamic shuttling of TIA-1 accompanies the recruitment of mRNA to mammalian stress granules. *J. Cell. Biol.* **151**, 1257-1268 (2000).

6. Wheeler, J. R., Matheny, T., Jain, S., Abrisch, R. & Parker, R. Distinct stages in stress granule assembly and disassembly. *Elife* **5** (2016).

7. Kedersha, N., Ivanov, P. & Anderson, P. Stress granules and cell signaling: more than just a passing phase? *Trends Biochem. Sci.* **38**, 494-506 (2013).

8. Buchan, J. R., Kolaitis, R. M., Taylor, J. P. & Parker, R. Eukaryotic stress granules are cleared by autophagy and Cdc48/VCP function. *Cell* **153**, 1461-1474 (2013).

9. Wippich, F. et al. Dual specificity kinase DYRK3 couples stress granule condensation/dissolution to mTORC1 signaling. *Cell* **152**, 791-805 (2013).

10. Berchtold, D., Battich, N. & Pelkmans, L. A Systems-Level Study Reveals Regulators of Membrane-less Organelles in Human Cells. *Mol. Cell* **72**, 1035-1049 e1035 (2018).

11. Zhang, K. et al. Stress Granule Assembly Disrupts Nucleocytoplasmic Transport. *Cell* **173**, 958-971 e917 (2018).

12. Shin, Y. & Brangwynne, C. P. Liquid phase condensation in cell physiology and disease. *Science* **357** (2017).

13. Wolozin, B. & Ivanov, P. Stress granules and neurodegeneration. *Nat. Rev. Neurosci.* **20**, 649-666 (2019).

14. Eiermann, N., Haneke, K., Sun, Z., Stoecklin, G. & Ruggieri, A. Dance with the Devil: Stress Granules and Signaling in Antiviral Responses. *Viruses* **12** (2020).

15. White, J. P. & Lloyd, R. E. Regulation of stress granules in virus systems. *Trends Microbiol.* **20**, 175-183 (2012).

16. Nover, L., Scharf, K. D. & Neumann, D. Formation of cytoplasmic heat shock granules in tomato cell cultures and leaves. *Mol. Cell. Biol.* **3**, 1648-1655 (1983).

17. Jain, S. et al. ATPase-Modulated Stress Granules Contain a Diverse Proteome and Substructure. *Cell* **164**, 487-498 (2016).

18. Aulas, A. et al. Stress-specific differences in assembly and composition of stress granules and related foci. *J. Cell. Sci.* **130**, 927-937 (2017).

19. Grousl, T., Vojtova, J., Hasek, J. & Vomastek, T. Yeast stress granules at a glance. *Yeast* **39**, 247-261 (2022).

20. Souquere, S. et al. Unravelling the ultrastructure of stress granules and associated P-bodies in human cells. *J. Cell Sci.* **122**, 3619-3626 (2009).

21. Uversky, V. N. Intrinsically disordered proteins in overcrowded milieu: Membrane-less organelles, phase separation, and intrinsic disorder. *Curr. Opin. Struct. Biol.* **44**, 18-30 (2017).

22. Markmiller, S. et al. Context-Dependent and Disease-Specific Diversity in Protein Interactions within Stress Granules. *Cell* **172**, 590-604 e513 (2018).

23. Padron, A., Iwasaki, S. & Ingolia, N. T. Proximity RNA Labeling by APEX-Seq Reveals the Organization of Translation Initiation Complexes and Repressive RNA Granules. *Mol. Cell* **75**, 875-887 e875 (2019).

24. Ohn, T., Kedersha, N., Hickman, T., Tisdale, S. & Anderson, P. A functional RNAi screen links O-GlcNAc modification of ribosomal proteins to stress granule and processing body assembly. *Nat. Cell. Biol.* **10**, 1224-1231 (2008).

25. Kato, M. et al. Cell-free formation of RNA granules: low complexity sequence domains form dynamic fibers within hydrogels. *Cell* **149**, 753-767 (2012).

26. Freibaum, B. D., Messing, J., Yang, P., Kim, H. J. & Taylor, J. P. High-fidelity reconstitution of stress granules and nucleoli in mammalian cellular lysate. *J. Cell. Biol.* **220** (2021).

27. Wheeler, J. R., Jain, S., Khong, A. & Parker, R. Isolation of yeast and mammalian stress granule cores. *Methods* **126**, 12-17 (2017).

28. Moller, H. D., Parsons, L., Jorgensen, T. S., Botstein, D. & Regenberg, B. Extrachromosomal circular DNA is common in yeast. *Proc. Natl. Acad. Sci. U. S. A.* **112**, E3114-3122 (2015).

29. Paulsen, T., Kumar, P., Koseoglu, M. M. & Dutta, A. Discoveries of Extrachromosomal Circles of DNA in Normal and Tumor Cells. *Trends Genet.* **34**, 270-278 (2018).

30. Arrey, G., Keating, S. T. & Regenberg, B. A unifying model for extrachromosomal circular DNA load in eukaryotic cells. *Semin. Cell.Dev.Biol.* **128**, 40-50 (2022).

31. Holt, S., Arrey, G. & Regenberg, B. Did circular DNA shape the evolution of mammalian genomes? *Trends Biochem Sci* **48**, 317-320 (2023).

32. Namkoong, S., Ho, A., Woo, Y. M., Kwak, H. & Lee, J. H. Systematic Characterization of Stress-Induced RNA Granulation. *Mol. Cell* **70**, 175-187 e178 (2018).

33. Ohi, M., Li, Y., Cheng, Y. & Walz, T. Negative Staining and Image Classification - Powerful Tools in Modern Electron Microscopy. *Biol. Proced. Online* **6**, 23-34 (2004).

34. Khong, A. et al. The Stress Granule Transcriptome Reveals Principles of mRNA Accumulation in Stress Granules. *Mol. Cell* **68**, 808-820 e805 (2017).

35. Iida, K., Suzuki, N., Sasaki, A., Ishida, S. & Arai, T. Development of a novel light-up probe for detection of G-quadruplexes in stress granules. *Sci. Rep.* **12**, 12892 (2022).

36. Kharel, P. et al. Stress promotes RNA G-quadruplex folding in human cells. *Nat. Commun.* **14**, 205 (2023).

37. Rodriguez, R. et al. A novel small molecule that alters shelterin integrity and triggers a DNA-damage response at telomeres. *J. Am. Chem. Soc.* **130**, 15758-15759 (2008).

38. Arthanari, H., Basu, S., Kawano, T. L. & Bolton, P. H. Fluorescent dyes specific for quadruplex DNA. *Nucleic Acids Res.* **26**, 3724-3728 (1998).

39. Ashe, M. P., De Long, S. K. & Sachs, A. B. Glucose depletion rapidly inhibits translation initiation in yeast. *Mol. Biol. Cell* **11**, 833-848 (2000).

40. Mateju, D. et al. Single-Molecule Imaging Reveals Translation of mRNAs Localized to Stress Granules. *Cell* **183**, 1801-1812 e1813 (2020).

41. Trachman, R. J., 3rd et al. Structure and functional reselection of the Mango-III fluorogenic RNA aptamer. *Nat. Chem. Biol.* **15**, 472-479 (2019).

42. Moon, S. L. et al. Multicolour single-molecule tracking of mRNA interactions with RNP granules. *Nat. Cell. Biol.* **21**, 162-168 (2019).

43. Sinclair, D. A. & Guarente, L. Extrachromosomal rDNA circles--a cause of aging in yeast. *Cell* **91**, 1033-1042 (1997).

44. Hull, R. M. & Houseley, J. The adaptive potential of circular DNA accumulation in ageing cells. *Curr. Genet.* **66**, 889-894 (2020).

45. Zhao, Y., Yu, L., Zhang, S., Su, X. & Zhou, X. Extrachromosomal circular DNA: Current status and future prospects. *Elife* **11** (2022).

46. Gomar-Alba, M. & Mendoza, M. Modulation of Cell Identity by Modification of Nuclear Pore Complexes. *Front. Genet.* **10**, 1301 (2019).

47. Panagaki, D. et al. Nuclear envelope budding is a response to cellular stress. *Proc. Natl. Acad. Sci. U. S. A.* **118** (2021).

48. Wu, S. et al. Circular ecDNA promotes accessible chromatin and high oncogene expression. *Nature* **575**, 699-703 (2019).

49. Shin, J. H. & Kelman, Z. The replicative helicases of bacteria, archaea, and eukarya can unwind RNA-DNA hybrid substrates. *J. Biol. Chem.* **281**, 26914-26921 (2006).

50. Raisner, R. M. et al. Histone variant H2A.Z marks the 5' ends of both active and inactive genes in euchromatin. *Cell* **123**, 233-248 (2005).

51. Santos-Pereira, J. M. & Aguilera, A. R loops: new modulators of genome dynamics and function. *Nat. Rev. Genet.* **16**, 583-597 (2015).

52. Niehrs, C. & Luke, B. Regulatory R-loops as facilitators of gene expression and genome stability. *Nat. Rev. Mol. Cell. Biol.* **21**, 167-178 (2020).

53. Dequeker, B. J. H. et al. MCM complexes are barriers that restrict cohesin-mediated loop extrusion. *Nature* **606**, 197-203 (2022).

54. Kuznetsov, V. A., Bondarenko, V., Wongsurawat, T., Yenamandra, S. P. & Jenjaroenpun, P. Toward predictive R-loop computational biology: genome-scale prediction of R-loops reveals their association with complex promoter structures, G-quadruplexes and transcriptionally active enhancers. *Nucleic Acids Res.* **46**, 7566-7585 (2018).

55. Miller, K. N. et al. Cytoplasmic DNA: sources, sensing, and role in aging and disease. *Cell* **184**, 5506-5526 (2021).

56. Hofmann, S., Kedersha, N., Anderson, P. & Ivanov, P. Molecular mechanisms of stress granule assembly and disassembly. *Biochim. Biophys. Acta Mol. Cell. Res.* **1868**, 118876 (2021).

57. Ben-Shem, A. et al. The structure of the eukaryotic ribosome at 3.0 A resolution. *Science* **334**, 1524-1529 (2011).

58. Hardy, S. J. S., Kurland, C. G., Voynow, P, Mora, G. The Ribosomal Proteins of Escherichia coli. I. Purification of the 30S Ribosomal Proteins. *Biochemistry* **8**, 2897-2905 (1969).

59. Vladimirov, S. N. et al. Characterization of the human small-ribosomal-subunit proteins by N-terminal and internal sequencing, and mass spectrometry. *Eur. J. Biochem.* **239**, 144-149 (1996).

60. Bailey, T. L., Johnson, J., Grant, C. E. & Noble, W. S. The MEME Suite. *Nucleic Acids Res.* **43**, W39-49 (2015).

61. Hanasaki, M. & Masumoto, H. CRISPR/Transposon gene integration (CRITGI) can manage gene expression in a retrotransposon-dependent manner. *Sci. Rep.* **9**, 15300 (2019).

62. Fischer, U., Huber, J., Boelens, W. C., Mattaj, I. W. & Luhrmann, R. The HIV-1 Rev activation domain is a nuclear export signal that accesses an export pathway used by specific cellular RNAs. *Cell* **82**, 475-483 (1995).

63. Ryan, O. W. et al. Selection of chromosomal DNA libraries using a multiplex CRISPR system. *Elife* **3** (2014).

64. Ferre-D'Amare, A. R., Zhou, K. & Doudna, J. A. Crystal structure of a hepatitis delta virus ribozyme. *Nature* **395**, 567-574 (1998).

65. Soni, R., Carmichael, J. P. & Murray, J. A. Parameters affecting lithium acetate-mediated transformation of Saccharomyces cerevisiae and development of a rapid and simplified procedure. *Curr. Genet.* **24**, 455-459 (1993).

66. Tripp, J. D., Lilley, J. L., Wood, W. N. & Lewis, L. K. Enhancement of plasmid DNA transformation efficiencies in early stationary-phase yeast cell cultures. *Yeast* **30**, 191-200 (2013).

Materials availability

Plasmids generated in this study are available from the authors under a material transfer agreement with Addgene. Requests should be submitted by email to A.R.F.

Data availability

Raw sequencing data have been deposited in the Sequence Read Archive (accession numbers for RNA part: SAMN33615213; SAMN33615214; SAMN33615215, SAMN33615216; accession numbers for DNA part: SAMN33683728; SAMN33683729; SAMN33683730; SAMN33683731; SAMN33683732; SAMN33683733; SAMN33683734; SAMN33683735; SAMN33683736; SAMN33683737; SAMN33683738; SAMN33683739; SAMN33683740). Requests for proteomics raw data should be submitted by email to A.R.F.

Acknowledgments We thank Drs. G. Piszceck and D. Wu of the Biophysics Core of the National Heart, Lung, and Blood Institute (NHLBI) for assistance in characterization of the purified stress

granule cores; D. Malide and X. Wu of the Light Microscopy Core (NHLBI) for stimulated emission depletion and confocal microscopy support; the staff of the Electron Microscopy Core (NHLBI) for technical assistance; M. Gucek and S. Patel of the Proteomics Core (NHLBI) for mass spectrometric analyses; and T. Dever (National Institute of Child Health and Human Development), H. Shroff (Janelia Research Campus),T. Tsukiyama (Fred Hutchinson Cancer Research Center), and C. Jones and all other members of the Ferré-D'Amaré laboratory for discussions. This work was supported by the intramural program of the NHLBI, National Institutes of Health, USA.

Authors contributions Study conceived and designed by N.A.D. and A.R.F. Experiments carried out by N.A.D. Data analyzed by N.A.D. and A.R.F. Manuscript written by N.A.D. and A.R.F.

Competing interests Authors declare no competing interests.